Application of unimolecular reaction rate theory for highly flexible transition states to the dissociation of CH_2CO into CH_2 and CO

Stephen J. Klippenstein
Arthur Amos Noyes Laboratory of Chemical Physics, California Institute of Technology, Pasadena, California 91125 and Department of Chemistry and Biochemistry, University of Colorado, Boulder, Colorado 80309-0215

R. A. Marcus
Arthur Amos Noyes Laboratory of Chemical Physics, California Institute of Technology, Pasadena, California 91125[a)]

(Received 21 October 1988; accepted 12 May 1989)

A previously described implementation of Rice–Ramsberger–Kassel–Marcus (RRKM) theory for unimolecular dissociation processes involving a highly flexible transition state is applied to the dissociation of CH_2CO into CH_2 and CO. Results of theoretical calculations for the energy and angular momentum resolved rate constants are presented. Using an added dynamical approximation, the product vibrational–rotational distributions are also calculated. The calculated rate constants are compared with the corresponding experimentally determined quantities where possible. Comparison is also made with phase space theory (PST). The RRKM-based calculations are in good agreement with both the experimentally determined rate constants of Zewail and co-workers and the experimentally determined photofragment excitation spectra of Moore and co-workers. The results on rates are in contrast to the corresponding results from PST calculations. The RRKM-based theory for the product vibrational–rotational distributions predicts a moderately greater probability for vibrational excitations than does PST (particularly for excess energies just above the threshold for excitation of a particular vibrational mode of the products). In other respects the RRKM-based predictions of the ro-vibrational product state distributions are quite similar to those of PST.

I. INTRODUCTION

Energy and partially angular momentum resolved rate constants and/or vibrational–rotational product state distributions have recently been obtained for a variety of unimolecular dissociations. These include the dissociations of NCNO,[1,2] H_2O_2,[3,4] CH_2CO,[5–8] and $C_6H_6^+$.[9] Such increasingly detailed experimental studies provide important examples for determining the validity of statistical theories and their implementation.

The dissociation of ketene into singlet methylene and carbon monoxide ($CH_2CO \rightarrow {}^1CH_2 + CO$) provides a nice example of the detailed experimental information that may now be obtained for unimolecular dissociation reactions. Zewail and co-workers[7] have used picosecond photofragment spectroscopy to determine the microcanonical unimolecular dissociation rate constants for a rotationally cold (≈ 3 K) distribution of CH_2CO molecules for excess energies ranging from 1100 to 5600 cm^{-1}. Moore and co-workers have used photofragment excitation spectroscopy to study the nascent product state distributions for excess energies ranging from 0 to 350 cm^{-1} [5,6] and subsequently for excess energies ranging from 1300 to 3000 cm^{-1}.[8] In addition, Moore *et al.*[10,11] have also used vacuum UV laser induced fluorescence experiments to determine the product state distributions resulting from the photodissociation of room temperature distributions of ketene molecules (excess energy above the singlet threshold of 2365 cm^{-1} plus thermal energy).

Moore and co-workers[5,6] have compared their experimental data on product state distributions for low excess energies (i.e., excess energies not exceeding any vibrational excitation thresholds) with phase space theory (PST)[12] and found that PST yields good agreement for the rotational state distribution. However, PST has been found to give, for other systems, less successful descriptions of either the dissociation rate constant or the vibrational–rotational distribution at higher excess energies.[1,13–17] Any hindered rotational motion of the two fragments at the transition state is omitted in PST and this omission can result in the prediction of too large a rate constant.[13–19] Moore and co-workers[5,6] have also compared their experimental results for these low excess energy product state distributions with the adiabatic channel model[20] (ACM), which includes the hindered rotational motion using some exponential interpolation formulas. In this comparison they found that, for the usual values of the universal interpolation parameter used for the ACM, the agreement of the calculated product state distributions with experiment was not as good as that for PST.

In the present article a previously described[18,19] method for implementing Rice–Ramsberger–Kassel–Marcus (RRKM) theory will be applied to the theoretical study of the CH_2CO dissociation. This method[13,18,19] treats the hindered rotational motions of the two separating fragments using classical phase space integrals for motion on a given

[a)] Contribution No. 7851.

 0021-9606/89/162280-13$02.10

potential energy surface. In contrast, PST treats these motions as free rotors. In the method[13,18,19] a Monte Carlo integration of the phase space integral for the number of states at the transition state is written as a convolution of a quantum number of states for the "conserved" modes and a classical density of states for the "transitional" modes, subject to a given energy E and total angular momentum quantum number J.

The theory used here has been described[18,19] and applied[16,17] previously and so will not be discussed further. The relative contributions of the singlet and triplet states of CH_2CO to the dissociation dynamics is considered briefly in Sec. II. The functional form of the model potential surface used is similar to that of Ref. 16 and is described briefly in Sec. III. The results of both the variational RRKM calculations and the PST calculations for the rate constants are presented and discussed in Sec. IV. A comparison with the experimental results of Zewail and co-workers[7] for the rate constants is also given there. Predictions of the overall vibrational–rotational product state distributions from both the RRKM-based theory of Ref. 21 and from PST are given in Sec. V for a variety of energies. Also given there is a comparison of RRKM-based and PST calculations of the room temperature thermally averaged CO vibrational excitation probability with the experimentally determined quantity of Nesbitt *et al.*[10] Also, in Sec. VI results on the experimental photofragment excitation spectra in Refs. 5 and 6 are discussed in terms of the RRKM-based theory and PST. In an additional calculation presented in Sec. VI, the triplet rate constant determined indirectly by Moore and co-workers[5,6] is considered. Concluding remarks are made in Sec. VII.

II. SINGLET/TRIPLET CONTRIBUTIONS

A schematic diagram of the low-lying electronic states for ketene is given in Fig. 1. (This figure has been taken from Ref. 5 and is based on the results of the *ab initio* calculations of Allen and Schaefer.[22]) The ketene photofragmentation occurs through first a photoexcitation to the S_1 state followed by either an internal conversion to the S_0 state or an intersystem crossing to the T_1 state. Dissociation then occurs in either the S_0 or T_1 state. The T_1 triplet state in Fig. 1 correlates to a product state $^3CH_2 + CO$ which is about 3150 cm^{-1} below the product state $^1CH_2 + CO$ to which the singlet state correlates.[23] The ketene triplet state has a barrier, with experiments suggesting[5] that this barrier is less than about 1500 cm^{-1}.

At low enough excess energies (i.e., at and below the threshold for the singlet products) the dissociation must of course occur only on the triplet potential energy surface. At energies slightly above the threshold for production of the singlet products competing dissociations occur in both the S_0 and T_1 states. In the photofragment excitation spectroscopy experiment of Ref. 5, Moore and co-workers found that the singlet/triplet branching ratio increases from 0 to 2 in the first 125 cm^{-1} above the singlet threshold. At a higher excess energy of 2365 cm^{-1} above the singlet threshold, no triplet product was observed in either the molecular beam study of Hayden *et al.*[24] or the vacuum UV laser induced fluorescence study of Nesbitt *et al.*[10] Thus, on the basis of

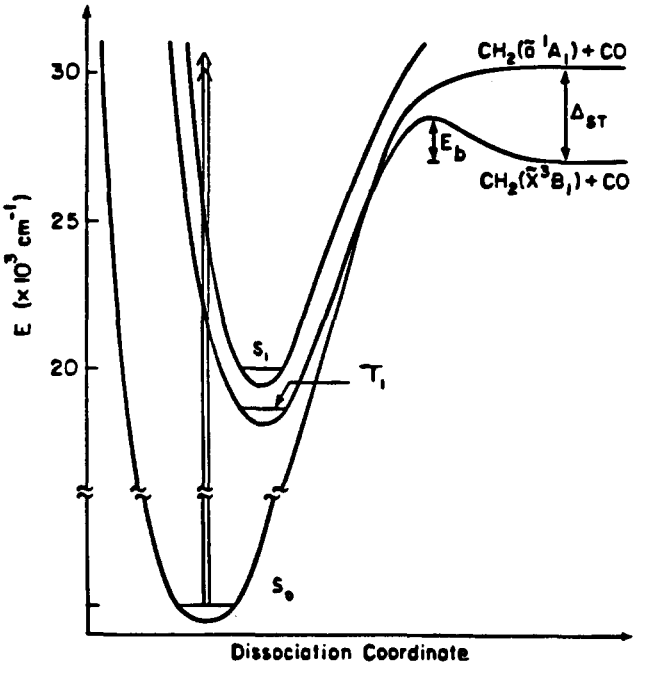

FIG. 1. Schematic potential energy diagram for the dissociation of CH_2CO into CH_2 and CO (taken from Ref. 5).

estimates of experimental detection sensitivity, the singlet-triplet branching ratio is at least $10^{5,10,24}$ for this higher excess energy.

The above experimental results indicate that the dissociation process changes fairly rapidly (within at least the first 2500 cm^{-1} above the singlet threshold) from being dominated by the triplet surface to being dominated by the singlet surface as the excess energy rises above the threshold for dissociation to singlet products. This fairly rapidly rising dominance of the singlet level suggests that a treatment which considers only the singlet state should be valid over a broad energy range. (For example, as indicated above, for energies over 125 cm^{-1} the singlet triplet branching ratios indicate that a treatment of only the singlet state should not introduce an error of more than 35% in the total rate constant, while for energies over 2500 cm^{-1} they indicate this error should not be greater than 10%.[5,10,24]) In the present article the results in Secs. IV and V are for the rate constants and product state distributions resulting from dissociation on only the singlet level. Additionally, all future values of excess energies in this article will be given relative to the threshold energy for production of singlet CH_2 in its lowest vibrational–rotational state. For the photofragment excitation spectra discussed in Sec. VI, again only the singlet state distributions are considered. However, the effect that the triplet state has on reducing the singlet quantum yields is also considered there.

III. POTENTIAL ENERGY SURFACES

A detailed potential energy surface for the transition state region is not available, and a model surface similar to those used previously in Refs. 13, and 16–18 is employed instead. (Eventually it is hoped that a detailed *ab initio* surface will become available. The present calculations can help

determine the particularly relevant ranges of coordinates for such a study. In particular, R † the center-of-mass to center-of-mass separation distance at the transition state was found to vary from about 2.6 to 3.4 Å in the present calculation.) The model potential surface for the transitional modes is taken to be the sum of a bonding potential for the dissociating C=C bond and a nonbonding potential for the remaining interfragment interactions. The intrafragment vibrational interactions correspond to the conserved modes and are represented by interpolation formulas rather than by a detailed potential energy surface.

The bonding potential is approximated by an effective Varshni potential multiplied by an orientation factor which accounts for the loss of bonding which occurs when the two fragments are improperly oriented. The orientation factor is chosen to be $\cos^2(\delta\theta_{CCO}[\cos^2(\delta\theta_{HCC_1}) + \cos^2(\delta\theta_{HCC_2})]/2$ when all three of $|\delta\theta_{CCO}|$, $|\delta\theta_{HCC_1}|$, and $|\delta\theta_{HCC_2}|$ are less than $\pi/2$ and zero otherwise.[25] Here, $\delta\theta_{CCO}$, $\delta\theta_{HCC_1}$, and $\delta\theta_{HCC_2}$ denote the deviations of the CCO and the two HCC bending angles from their corresponding equilibrium values. The equilibrium values for these and other coordinates together with certain other spectroscopic parameters used here may be found in Table I.

An effective Varshni potential[31] is given by the standard form

$$V_V^{\text{eff}} = D_{CC}^{\text{eff}}\left\{1-\left(\frac{r_{CC}^{e,\text{eff}}}{r_{CC}}\right)\exp\left[-\beta_{CC}^{\text{eff}}(r_{CC}^2 - r_{CC}^{e,\text{eff}^2})\right]\right\}^2 - D_{CC}^{\text{eff}}. \quad (1)$$

The quantities D_{CC}^{eff}, and $r_{CC}^{e,\text{eff}}$ correspond to the effective C=C dissociation energy and separation distance, respectively, while, here β_{CC}^{eff} is related to the C=C force constant and to the other interactions, as is D_{CC}^{eff}: The parameters for this surface, given in Table II, were determined through a fit of the total potential energy (including the nonbonding interactions) to the set of assumed Varshni parameters, β_{CC}, D_{CC}, and r_{CC}^e. These assumed Varshni parameters in turn were obtained from a consideration of the spectroscopically determined force constant,[27] dissociation energy,[5] and separation distance.[27] This fit of the potential surface was performed for a center-of-mass to center-of-mass separation R in the interval of 2.8–3.0 Å.[32]

The nonbonding potential was taken as the sum of the van der Waals interactions between the nonbonded atoms, with the van der Waals interactions represented by Lennard-Jones 6-12 potentials,

$$V_{LJ} = \sum_{i=1}^{3}{}' \sum_{j=1}^{2}{}' 4\epsilon_{ij}\left[\left(\frac{\sigma_{ij}}{r_{ij}}\right)^{12} - \left(\frac{\sigma_{ij}}{r_{ij}}\right)^{6}\right], \quad (2)$$

where i and j label the atoms in the CH_2 and CO fragments, respectively, and the prime indicates that the C=C bond is not included in the sum. The parameters σ_{ij} and ϵ_{ij} denote the usual Lennard-Jones parameters for the interaction between atoms i and j while r_{ij} is the separation distance between atoms i and j. The Lennard-Jones parameters used here were taken from Ref. 33 and are given in Table III.

In the current absence of a detailed potential energy surface the conserved modes were treated as quantum oscillators using an exponential interpolation[13,20] between the parameters describing the reactants and the products, given by

$$\lambda_i(R) = \lambda_i^p + (\lambda_i^r - \lambda_i^p)g(R), \quad (3)$$

where $g(R) = \exp[-\alpha(R - R^e)]$.[13,20] The quantity λ denotes a frequency ν, equilibrium bond separation distance r^e, and equilibrium bending angle θ^e, for the given atoms, and i denotes CH, CO, or HCH. The r and p superscripts denote the reactant (CH_2CO) and products ($^1CH_2 + CO$), respectively. The harmonic parameters for the conserved modes are given, together with the other spectroscopic parameters, in Table I. Apart from the calculation of the density states, the CO stretch and CH_2 scissor were treated as Morse oscillators, with the two Morse parameters determined via a fit to the fundamental and first overtone frequencies of the products. This was necessary in order to obtain the correct term values for the product $v = 2$ states of these oscillators. The anharmonicities were then assumed to be the same for both the reactants and the products. The ratio of the statistical factor for the reactants to that for the transition state is unity.

TABLE I. Spectroscopic parameters for $CH_2CO \rightarrow {}^1CH_2 + CO$.

Parameter		Reactants[a] value	Products[b] value
Frequencies (cm^{-1})	CH asym stretch	3166	2864
	CH sym stretch	3070	2806
	CO stretch	2152	2143
	CH_2 scissor	1388	1352
	CC stretch	1118	
	CH_2 rock	977	
	CH_2 wag	591	
	CCO bend	525	
	CCO bend	438	
Rotational constants (cm^{-1})	A_{CH_2CO/CH_2}	9.41	20.14
	B_{CH_2CO/CH_2}	0.344	11.20
	C_{CH_2CO/CH_2}	0.331	7.07
	B_{CO}		1.93
Coordinates	R_e	2.054 Å	
	$r_{e,CH}$	1.077 Å	1.11 Å
	$r_{e,CO}$	1.161 Å	1.128 Å
	θ_{HCH}^e	122.0°	102.0°
	θ_{CCO}^e	180°	

[a] The parameters for the reactants have been obtained from Refs. 26 and 27.
[b] The parameters for the products have been obtained from Refs. 28–30.

TABLE II. Varshni potential parameters for CH_2CO.

Parameter	Assumed potential[a]	Effective potential
$r_{e,CC}$	1.316 Å	1.15 Å
β_{CC}	0.73 $Å^{-2}$	0.7765 $Å^{-2}$
D_{CC}	32 304 cm^{-1}	61 500 cm^{-1}

[a] The parameter β_{CC} was obtained by setting $d^2V_{varsh}/dr_{CC}^2 = k$, where k is the force constant for the central CC stretch given in Ref. 27.

TABLE III. Lennard-Jones potential parameters for CH_2CO.

Parameter	Value[a]	Units
σ_{CO}	3.36	Å
σ_{CH}	3.40	Å
σ_{OH}	3.00	Å
ϵ_{CO}	56.	cm^{-1}
ϵ_{CH}	11.	cm^{-1}
ϵ_{OH}	13.	cm^{-1}

[a] All values have been obtained from Ref. 33, by making use of the combination rules $\epsilon_{ij} = (\epsilon_{ii}\epsilon_{jj})^{1/2}$ and $\sigma_{ij} = \frac{1}{2}(\sigma_{ii} + \sigma_{jj})$.

The value of the exponential interpolation parameter α used here was 1.8 $Å^{-1}$. Calculations were also performed with values of 1.2 and 1.0 $Å^{-1}$ for α. It was found that the results for the latter two values of α were very similar to those obtained with the present value of 1.8 $Å^{-1}$. The only differences were (i) a decrease in the total number of states by a factor of about 20% for the lower α values, and (ii) decreased vibrational excitation probabilities for energies very near the excitation threshold. Otherwise, the results were nearly independent of this variation in α. The need for a value of α larger than 1.0 $Å^{-1}$ can be understood when one considers that the value for α is often assumed to be given by about 0.5 times the Morse β parameter.[20] In that case the estimated α value would be 1.8 $Å^{-1}$.

The density of states for the reactant at a given energy and total angular momentum was obtained from the Whitten–Rabinovitch formula using the harmonic frequencies given in Table I. The contribution of anharmonicities and mode–mode coupling to the density of states is assumed for the present to be small (i.e., less than a factor of about 1.5[34]) and nearly constant over the energy range to be considered. Additionally, the correction factor is the same for both the variational RRKM and the PST calculations to be presented.

The Monte Carlo error bars for all of the variational RRKM calculations presented here are on the order of $\pm$ 5% to 10%. A brief description of the present quantum PST calculations is given in the Appendix, together with specific details pertaining to the present CH_2CO dissociation reaction.

IV. RATE CONSTANTS

A. Results

The expression for the RRKM rate constant at a given energy E and total angular momentum quantum number J is given by

$$k_{EJ} = \frac{N^{\dagger}_{EJ}}{h\rho_{EJ}}, \tag{4}$$

where $N^{\dagger}_{EJ}$ is the number of states at the transition state of given J, with an energy equal to or less than E, and ρ_{EJ} is the density of states for the reactant with given E and J. The $N^{\dagger}_{EJ}$ is determined variationally.

$$N^{\dagger}_{EJ} = \min N_{EJ}(R) \qquad (R_0 \leqslant R \leqslant \infty), \tag{5}$$

where R_0 is some minimum R considered and is taken here to be 2.4 Å. In the expression in Eq. (4) energy and angular momentum are taken to be the only conserved quantities. The effect of conservation of nuclear spin and parity with respect to inversion is considered in the Appendix. In the present section various expressions for N_{EJ} will be considered and the resultant rate constants compared with the experimentally determined rate constants of Zewail and co-workers.[7]

First, we consider the distribution of initial total angular momentum J of the ketene molecules. The experimental rate constants have been obtained through photoexcitation of a molecular beam of rotationally cold ketene molecules with $J \leqslant 2$.[7] We found, in calculations of k_{EJ} for $J = 1$ and 3, that the quantum PST results were nearly identical for these two J's, while the variational RRKM results were typically 20% higher for $J = 3$ than for $J = 1$. The fact that a slightly lower ($\approx$20%) k_{EJ} is obtained for $J = 1$ than for $J = 3$ in the RRKM calculations is probably due to a classical treatment of the rotational modes in the present RRKM method. (The difference between the k_{EJ}'s determined for $J = 1$ and $J = 3$ by a PST calculation in which the rotational modes were treated classically was nearly identical to the difference observed for the $J = 1$ and $J = 3$ RRKM theory calculations.) Since the present results for k_{EJ} are nearly independent of J in this range of J the calculation for a single value of J rather than for a thermal average (with a temperature of $\approx$3 K) over the initial distribution of J for ketene can be expected to give acceptable results. In summary, the results presented below are for a total angular momentum $J = 3$.

In Fig. 2 results from both the variational RRKM and the quantum PST calculations are given for k_{EJ} for dissociation on the S_0 surface, with the energies ranging from 100 to 6000 cm^{-1} above the singlet threshold. Also given there are the experimental results of Zewail and co-workers[7] for the rate constant for dissociation on the S_0 plus T_1 surfaces. The application of PST involves a choice of a C_6 potential parameter to describe the strength of the long range attractive po-

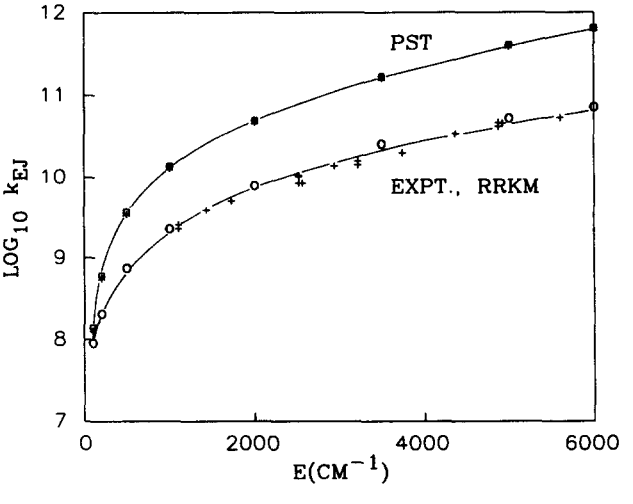

FIG. 2. Plot of calculated rate constant log k_{EJ} vs energy. The pluses denote the experimental results, the open circles the variational RRKM calculation, the filled boxes the quantum PST calculation, and the asterisks the classical PST calculation.

tential acting between the dissociating fragments. Moore and co-workers[5,6] found in their PST calculations that a very strongly attractive potential gave the best agreement with their experimentally determined photofragment excitation spectra and, thereby, that the C_6 parameter was constrained to be greater than 5×10^4 cm^{-1} Å^6. A $C_6=\infty$ value corresponds to having the phase space transition state at $R=\infty$ [the phase space transition state occurs where there is a maximum in the sum of the attractive potential $-C_6/R^6$ and the repulsive centrifugal potential $l(l+1)\hbar^2/2\mu R^2$]. For the PST results calculations were performed for C_6 values of both 5×10^4 and 10^{20} cm^{-1} Å^6. The PST calculations with these two different values for the C_6 parameter were within 6% of each other throughout the entire energy range considered here. For the PST results presented in Fig. 2 the latter value of the C_6 parameter was used.

It is also of interest to consider a PST calculation in which the rotational modes are treated classically rather than quantum mechanically, since this type of calculation is more immediately comparable with the present variational RRKM calculations. The use of $C_6=\infty$ in this type of PST calculation gives a number of states that is identical to the number of states at infinite separation, $N_{EJ}(\infty)$, determined from the present Monte Carlo phase space integral method. The results of calculations based on $N_{EJ}(\infty)$ are also given in Fig. 2. As is evident there, the k_{EJ}'s thus determined are typically 10%–20% smaller than those determined from quantum PST with the same C_6.

B. Discussion

From the results given in Fig. 2 it is seen that the RRKM k_{EJ}'s are in considerably better agreement with the experimental results than those of PST. Furthermore, the deviation between the variational RRKM k_{EJ}'s and the PST k_{EJ}'s rapidly increases with increasing energy: the ratio of the PST k_{EJ} result (in particular the RRKM result at $R^\dagger=\infty$) to the variational RRKM k_{EJ} increases from 1.3 to 8.0 as the excess energy E increases from 100 to 6000 cm^{-1}.

It is interesting to note that this deviation of the variationally determined RRKM k_{EJ}'s from the classical PST rates is considerably larger than that observed in the previous applications of this method to other molecules.[13,14,16,17] One reason for this behavior can be seen by comparing the Varshni β parameter for the assumed potential for CH_2CO with that for the previous applications. For NCNO, C_2H_6, CH_4, and H_2O_2 the β parameter is 0.48, 0.37, 0.47, and 0.61 Å^{-2}, respectively, whereas for CH_2CO the β parameter is 0.73 Å^{-2}. (β is obtained, it will be recalled, by setting the quantity d^2V_{Varsh}/dr^2 equal to the force constant for the stretching motion along r, with r being the bond separation distance for the bond which is being broken.) For H_2O_2 the β parameter of 0.61 is also quite large. However, other factors such as the relatively small van der Waals radii for H–H and O–H interactions may have served to reduce the deviation of the PST results from the variational RRKM results. In addition, the results for the H_2O_2 dissociation do have a larger deviation from PST than do those for the dissociation of NCNO and C_2H_6.[17] This larger value of β for ketene may reflect, in part, the fact that now the rupture of a double bond is involved, whereas, in the other molecules only a single bond was dissociating. One result of the large value of β is that the fragments come in closer contact before sensing the strong bonding attraction, thereby allowing the atom–atom repulsions between them (i.e., the van der Waals repulsions and the orbital angular momentum centrifugal repulsion) to be of larger magnitude. This effect leads to a hindered rotation and thereby to a smaller value for the number of states (phase space integral) N_{EJ} at the transition state, and hence a smaller k_{EJ} for the variational RRKM rate constant.

Another contributing factor to this quite large difference from PST is the asymmetry in the interaction potential as CH_2 rotates about its center of mass. When CH_2 rotates about its center of mass, the H atoms sweep out a relatively large volume. As a result strongly repulsive van der Waals interactions with the CO fragment occur for some phases of the rotation (hindered rotation), thereby, reducing the phase space integral.

One final point of interest concerns the possible effect of there being two minima in the plot of the number of states versus reaction coordinate. This effect was previously considered by the present authors for the dissociation of NCNO in Refs. 16 and 19. In the present case when considering the rate constants the inner minimum of N_{EJ} rapidly (i.e., within the first few hundred cm^{-1}) becomes the dominant minimum. Thus, the effect of the two minima will only be nonnegligible at energies very near the singlet threshold. The energies of interest experimentally are typically much higher (i.e., they range from about 1000 to about 6000 cm^{-1}). For these reasons a consideration of the effect of the two minima on the rate constants has not been given here. However, in a later publication it will be seen that the qualitative effect of the two minima on an RRKM-based calculation of photofragmentation spectra for vibrationally excited products can be nonnegligible.

V. PRODUCT STATE DISTRIBUTIONS

A. Results

RRKM theory was originally developed for the calculation of rate constants rather than for product state distributions. Because of the frequently strong interactions in the vicinity of the transition state, various dynamical effects may occur after the system leaves the transition state in RRKM theory, and some dynamical assumption is needed to apply an RRKM treatment to the product state distributions. Instead, product state distributions have frequently been calculated by experimentalists using PST. However, it has been found that although PST has been successfully used at subvibrational excitations of the products, the vibrational state distributions of the products predicted by PST theory have been lower than those observed experimentally.[1,10] Further, particularly at higher energies, PST gives too large a k_{EJ}.[13–15]

In Ref. 21 one explanation for this success of PST for calculating rotational distributions at subvibrational excitation energies but for being inaccurate for the k_{EJ}'s[13–15] was suggested: It was assumed in Ref. 21 that the motions of the conserved vibrations (i.e., those vibrational modes which retain their vibrational character in both the product and

reactant states), are largely adiabatic after passing through the variationally determined RRKM transition state, but the motions of the transitional degrees of freedom are not adiabatic. In this case only the vibrational distribution is postulated to be statistically determined by the number of states at $R^\dagger_i$, which is the RRKM transition state (minimum in the number of states) for the given vibrational state i. This vibrational motion is assumed to be adiabatic after that point. The transitional modes on the other hand (i.e., those modes which are rotational in nature in the product state) are assumed to continue their free interchange of energy after passing through $R = R^\dagger_i$, subject to total angular momentum conservation, until an $R = R_l$, the site of the orbital–angular momentum dependent barriers of PST, is reached. The subsequent motion involves no further internal interactions of the fragment. The rotational distributions are then given by the statistical quantum PST[12] distribution for the vibrational distribution determined from the given $R^\dagger_i$'s. The probability of obtaining a particular product vibrational–rotational state is now given by the product of the statistical RRKM probability for occupation of the vibrational state and the conditional quantum PST probability for occupation of the rotational state given that the vibrational state is already occupied.[21] The results reduce, in effect, to PST at energies below the threshold for product vibrational excitation.

Further details on this method for determining the vibrational–rotational distributions (including specific formulas for the above described probabilities) are given in Ref. 21. Calculations based on this method have been presented in Ref. 16 for the dissociation of NCNO into NC and NO. The procedure in the present calculations is the same as that described there with three further remarks:

First, two methods were available for determining the vibrational distribution,[16,21] one based on the calculation of the vibrational distribution at an overall $R^\dagger$, and the other based on using individual $R^\dagger_i$'s. In the overall total number of states N_{EJ} has its minimum at $R = R^\dagger$ and thus varies little with R for R near $R^\dagger$. However, the number of states for the particular vibrational state of interest N_{EJi} may instead be far from its minimum at $R = R^\dagger$ and then is rapidly varying with R in the neighborhood of $R^\dagger$. In this case, a small error in $R^\dagger$ can yield an appreciable error in N_{EJi}, and hence in the vibrational distribution, given by the ratio N_{EJi}/N_{EJ} at $R^\dagger$. For this reason, only the $R^\dagger_i$ method has been used in the calculations given in the present article for the product state distribution.

Second, in calculating the distributions one should also consider both the initial distribution of reactant states and the distribution of excited states resulting from the laser photoexcitation process. The procedure for doing this is analogous to that considered by Moore and co-workers[5] in their determination of theoretical photofragment excitation spectra. For completeness, a brief description of the procedure used here is given in the Appendix.

Last, the question of the effect of there being two minima in the plot of the number of states versus reaction coordinate again arises. As discussed in Refs. 16 and 19, one simple method for approximately accounting for this effect (when considering the rate constants) is to assume that these two minima correspond to two transition states acting in series. An assumption of statistical probabilities for crossing back and forth between the two "transition states" results in an effective number of states for the transition state which depends on the number of states at the two minima and at the maximum separating these two minima.[35,36]

$$N^\dagger_{EJ} = \frac{N^{\dagger 1}_{EJ} N^{\dagger 2}_{EJ}}{N^{\dagger 1}_{EJ} + N^{\dagger 2}_{EJ} - N^{\dagger 1}_{EJ} N^{\dagger 2}_{EJ}/N^{\max}_{EJ}}. \tag{6}$$

Typically, this effective number of states is used in the expression for the rate constant.[16,19,35,37] The Hirschfelder result in Ref. 35(b) gives the probability of reaction in terms of two transmission probabilities, one at each of the two transition states. If we now focus on a particular state i of the conserved modes and assume adiabaticity for the motion of that state in the region between the two minima, we need consider no transition between two different states of the conserved modes. In this case, the statistical reflection probabilities in Ref. 35(b), ρ_1 and ρ_2, now for the flux of this state i become $N^1_{EJ,i}/N^{\max}_{EJ,i}$ and $N^2_{EJ,i}/N^{\max}_{EJ,i}$, where $N^1_{EJ,i}$ and $N^2_{EJ,i}$ represent the number of states at the two minima in the flux and $N^{\max}_{EJ,i}$ represents the maximum in the number of states in between these two minima. One then obtains

$$N^\dagger_{EJ,i} = \frac{N^{\dagger 1}_{EJ,i} N^{\dagger 2}_{EJ,i}}{N^{\dagger 1}_{EJ,i} + N^{\dagger 2}_{EJ,i} - N^{\dagger 1}_{EJ,i} N^{\dagger 2}_{EJ,i}/N^{\max}_{EJ,i}}. \tag{7}$$

Equation (7) is used below to determine the product vibrational distribution.

We note that we are considering the product state distributions resulting from dissociation on the singlet surface only. (The product state distributions resulting from $^3CH_2$ may not be determined by the present methods, since they involve larger exit channel effects, due to the subsequent drop of the potential energy in the exit channel, cf. Fig. 1.) At energies below the threshold for vibrational excitation the predicted distributions for $^1CH_2$ are just those of PST.[16,21] However, at higher excess energies the present vibrational–rotational distributions can differ quite considerably from those of PST, since the vibrational distribution is determined at $R^\dagger_i$'s which are, typically, different from the loose transition state $R^\dagger$.

In Table IV results of calculations for the vibrational distribution are given for five different excess energies in the range 1500–3500 cm^{-1}. The present calculations were performed for a total angular momentum quantum number J of 1 and for a J of 3. The calculated vibrational distributions for $J = 3$ were within the Monte Carlo error bars of those for $J = 1$ at the same excess energy in all cases. Thus, once again the use of results for a single value of J, rather than for a thermal average over the initial distribution of ketene states at 3 K suffices. The product distributions presented in Table IV are for $J = 3$.

B. Discussion

It is seen in Table IV that the largest relative differences between the RRKM and PST calculations of the product state distributions arise for the calculated probability of excitation for excess energies which only slightly exceed the

TABLE IV. Vibrational distributions for CH_2CO at different excess energies.

Vibrational level $v_{CO}, v_{HCH}, v_{CH}^{sym}, v_{CH}^{asym}$	Excess energy (cm^{-1})	Vibrational distribution RRKM[a]	PST
0,0,0,0	1500	0.97(0.98)	0.99
0,1,0,0	1500	0.030(0.025)	0.0089
0,0,0,0	2000	0.86	0.91
0,1,0,0	2000	0.14	0.090
0,0,0,0	2500	0.74	0.82
0,1,0,0	2500	0.22	0.17
1,0,0,0	2500	0.037(0.035)	0.016
0,0,0,0	3000	0.65	0.72
0,1,0,0	3000	0.23	0.21
1,0,0,0	3000	0.091	0.058
0,2,0,0	3000	0.018	0.0081
0,0,1,0	3000	0.0074(0.0068)	0.0029
0,0,0,1	3000	0.0044(0.0037)	0.0014
0,0,0,0	3500	0.51	0.61
0,1,0,0	3500	0.25	0.22
1,0,0,0	3500	0.12	0.091
0,2,0,0	3500	0.054	0.033
0,0,1,0	3500	0.039	0.024
0,0,0,1	3500	0.031	0.020

[a] The numbers in parentheses have been determined via Eq. (7) which considers the effect of the two minima and have been given only where they differ from the result obtained using the absolute minimum of the two minima. Where only one figure is given there was effectively only one minimum.

threshold for vibrational excitation of a particular mode. The results in Table IV also indicate a slightly larger probability for population of excited vibrational states of other vibrational modes for RRKM theory as compared with PST. It should be cautioned that the calculated vibrational product distributions may be sensitive to the potential energy surface and that the present surface is only an approximate model. The development of an *ab initio* surface would be particularly desirable.

In Ref. 10 the experimental results showed that the CO vibrational distribution resulting from the dissociation of a room temperature thermal distribution was higher than that predicted by PST: In the initial thermal distribution of the ketene molecules the population of excited vibrational states is greater than 20% (e.g., as in Fig. 4 of Ref. 10). For these excited vibrational states the vibrational distribution calculated here is typically a factor of two or more larger than that for the ground vibrational state. This relatively larger population of excited vibrational states suggests that for a quantitative comparison of the present results with those of Ref. 10, the calculated product vibrational distribution must be averaged over the 300 K thermal vibrational–rotational distribution of ketene molecules. (Details of the thermal averaging procedure used are given in the Appendix.) The laser wavelength used in Ref. 10 corresponds to an excess energy of 2365 cm^{-1}. The results of this thermal averaging procedure for the excitation energy corresponding to this laser wavelength are given as follows.

The experimental result[10] for the ratio of populations in $v_{CO} = 1$ to $v_{CO} = 0$ was 0.09 ± 0.05 at an excess energy of 2365 cm^{-1}. Taking into account the initial thermal distribution of the ketene molecules, the PST value[10] was 0.013. Here, we calculate the PST value to be 0.026 and the variational RRKM result to be 0.043. This variational RRKM result is at the edge of the error bars given for the experimental value. The difference between the present and previous PST calculations may be due to a neglect previously[10] of the triangle inequality in J, k, and l, where k is the magnitude of the vector sum of the two fragment angular momenta, and to a possible emission in Ref. 10 of the correlation between the thermal energy and the total angular momentum. The k_{EJ}'s calculated from the present version of PST are, however, in agreement with those plotted in Fig. 8 of Ref. 6, taken from the same laboratory.

It is also of interest to consider the full vibrational–rotational distribution for excess energies exceeding the threshold for vibrational excitation and to note where the PST and RRKM results differ significantly. Such conditions would be useful for testing experimentally the cases where the predictions for the vibrational distributions are quite different in the two treatments, and so serve as a test of the assumptions therein, including those for the behavior in the exit channel. Again, there is the initial distribution of angular momentum for the reactant ketene molecules to be considered. Moore and co-workers[5,6] found that the rotational temperature of their cold beam of ketene molecules was 2.6 ± 0.8 K. The rotational distributions calculated below are based on a temperature of 3 K although the results were found not to depend too strongly on this temperature. A discussion of the thermal averaging procedure is given, as already noted, in the Appendix.

In Figs. 3–11 the vibrational–rotational distributions determined from the present variational RRKM-based calculations are compared with corresponding purely PST calculations. These distributions are given for three excess energies in the interval 1500–3500 cm^{-1}. (The small even–odd oscillations seen in the distributions presented in Figs. 3–11 are due to systematic fluctuations in the quantum PST number of states, perhaps because of angular momentum conser-

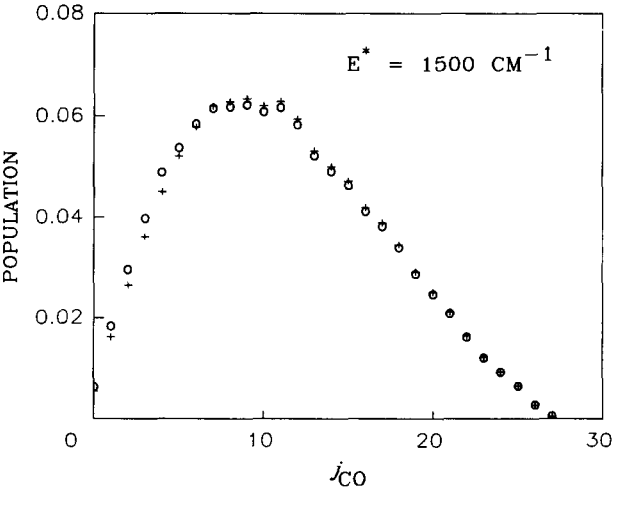

FIG. 3. Plot of CO rotational distribution for $v_{CO} = 0$, predicted by PST (pluses) and variational RRKM theory (circles) for an excess energy of 1500 cm^{-1}.

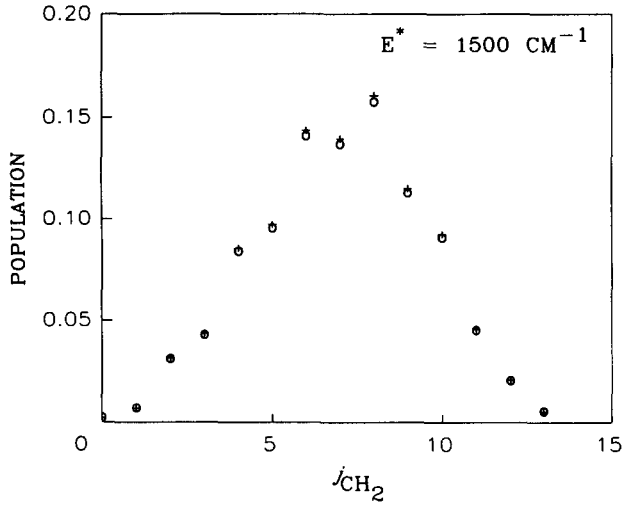

FIG. 4. Plot of CH_2 rotational distribution for $v_{HCH} = 0$, $v_{CH}^{sym} = 0$, $v_{CH}^{asym} = 0$, predicted by PST (pluses) and variational RRKM theory (circles) for an excess energy of 1500 cm^{-1}.

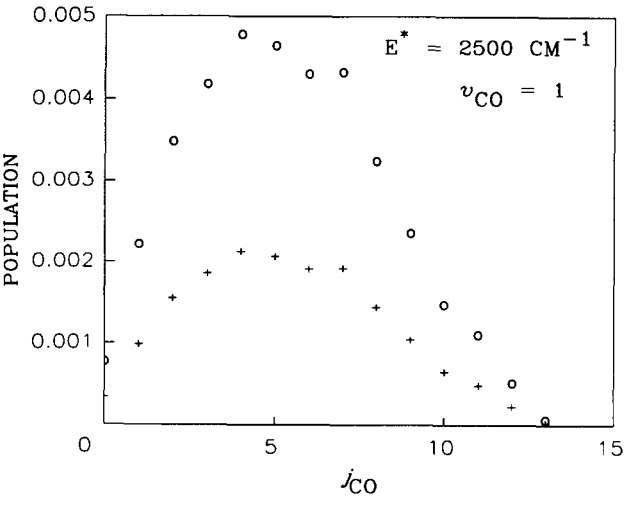

FIG. 7. Plot of CO rotational distribution for $v_{CO} = 1$, predicted by PST (pluses) and variational RRKM theory (circles) for an excess energy of 2500 cm^{-1}.

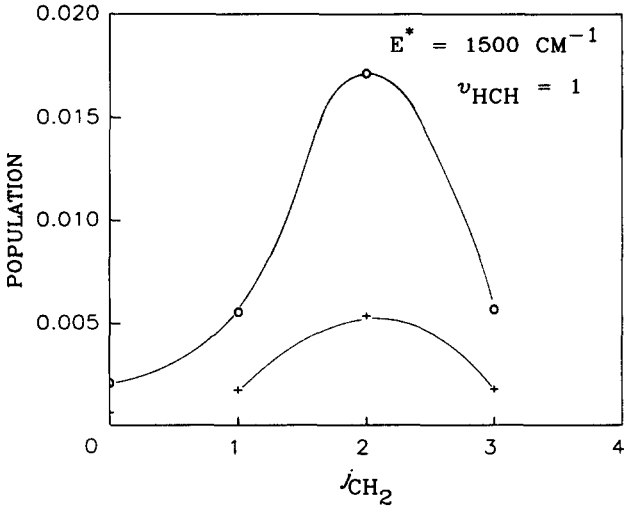

FIG. 5. Plot of CH_2 rotational distribution for $v_{HCH} = 1$, $v_{CH}^{sym} = 0$, $v_{CH}^{asym} = 0$, predicted by PST (pluses) and variational RRKM theory (circles) for an excess energy of 1500 cm^{-1}.

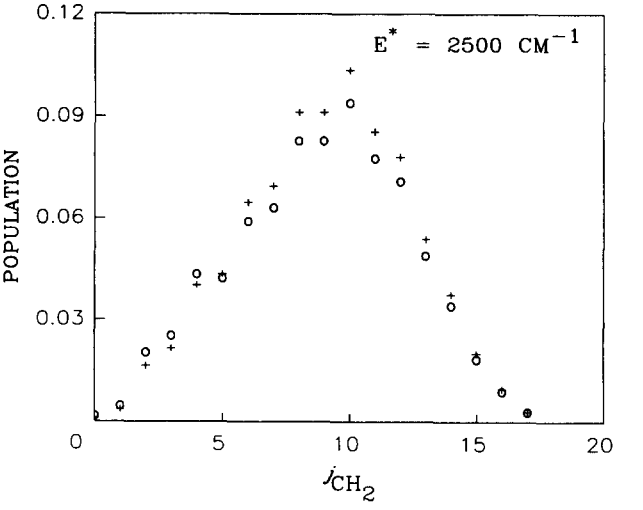

FIG. 8. Plot of CH_2 rotational distribution for $v_{HCH} = 0$, $v_{CH}^{sym} = 0$, $v_{CH}^{asym} = 0$, predicted by PST (pluses) and variational RRKM theory (circles) for an excess energy of 2500 cm^{-1}.

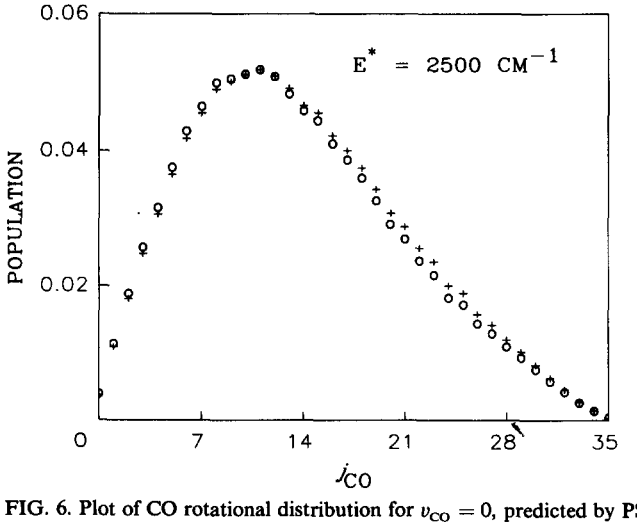

FIG. 6. Plot of CO rotational distribution for $v_{CO} = 0$, predicted by PST (pluses) and variational RRKM theory (circles) for an excess energy of 2500 cm^{-1}.

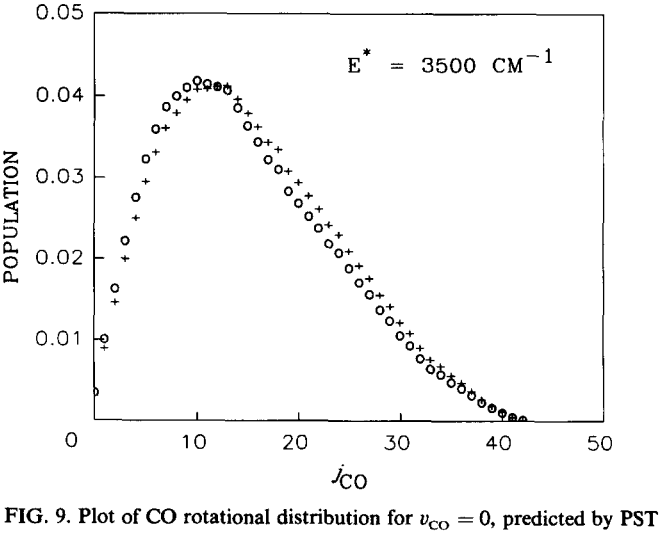

FIG. 9. Plot of CO rotational distribution for $v_{CO} = 0$, predicted by PST (pluses) and variational RRKM theory (circles) for an excess energy of 3500 cm^{-1}.

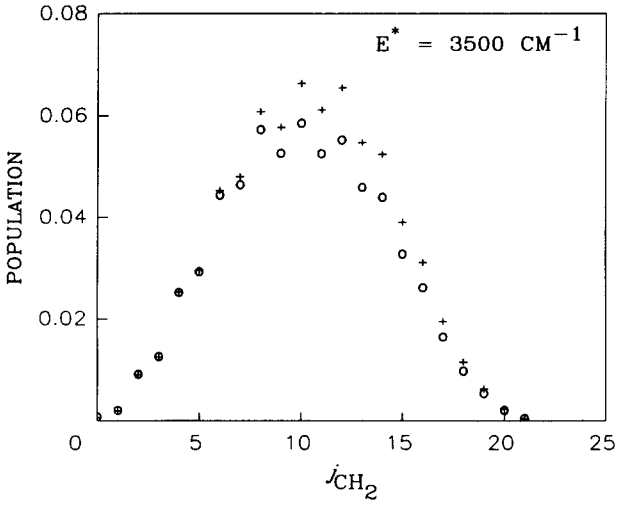

FIG. 10. Plot of CH_2 rotational distribution for $v_{HCH} = 0$, $v_{CH}^{sym} = 0$, $v_{CH}^{asym} = 0$, predicted by PST (pluses) and variational RRKM theory (circles) for an excess energy of 3500 cm^{-1}.

vation rules, and have no relation to the Monte Carlo error bars of the vibrational part of the calculation.) Even for the highest excess energy considered it appears that the RRKM and PST rotational distributions are quite similar. However, once again, in the RRKM-based treatment there is a predicted substantially increased vibrational excitation for all vibrational modes at excess energies slightly exceeding the threshold for their excitation. Other than these increased vibrational excitations, the only visible difference is in the rotational distributions for the $v = 0$ levels of both the CH_2 and CO fragments, where it is seen that in the RRKM-based calculations a slight shift of the distribution towards lower j states is predicted.

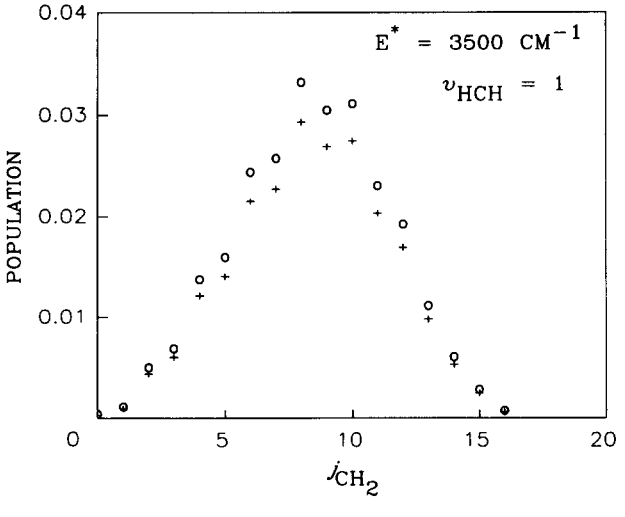

FIG. 11. Plot of CH_2 rotational distribution for $v_{HCH} = 1$, $v_{CH}^{sym} = 0$, $v_{CH}^{asym} = 0$, predicted by PST (pluses) and variational RRKM theory (circles) for an excess energy of 2500 cm^{-1}.

VI. PHOTOFRAGMENT EXCITATION SPECTRA

A. Results

In the photofragment excitation spectra of Moore and co-workers[5,6,8] the dependence on energy of a particular vibrational–rotational state of the CH_2 fragment is probed. The determination of theoretical photofragment excitation spectra has been described in Refs. 5 and 6, where it is noted that the calculation involves (1) the determination of the distribution of initial ketene vibrational–rotational states, (2) the determination of the rotational line strengths for the ketene photoexcitation process, and (3) the determination of the dissociation quantum yield for the rotational state of interest. The photofragment excitation experiments of Moore and co-workers in Refs. 5 and 6 were performed at excess energies well below the vibrational threshold. Thus, if the present RRKM-based method for determining the dissociation quantum yield is used to describe the photofragment excitation spectra of Refs. 5 and 6 at these energies the RRKM-based results are exactly the quantum PST results, which were described in Refs. 5 and 6, aside from the consideration of the singlet triplet branching ratio, discussed below. The results at higher excess energies where vibrational excitation of the products occurs will be discussed elsewhere.

B. Triplet rate constant

One further calculation involves an estimate of the triplet rate constant k_t, as follows. This calculation is based on a consideration of the quantum yield for a particular singlet state and its dependence on k_t. This quantum yield itself can be regarded as the product of two factors: (i) the probability for obtaining singlet states, $P(s)$, and (ii) the conditional probability for obtaining a particular nuclear spin vibrational–rotational n singlet state, given that the product is in the singlet state, $P(n|s)$. The first factor $P(s)$ is given by the ratio of the singlet rate constant to the sum of the singlet and triplet rate constants. In Ref. 5, PST was used to calculate the singlet rate constant and the quantity $P(n|s)$. As discussed in Ref. 5, a calculated photofragment excitation spectrum could then be determined by assuming some given value for the triplet rate constant. By comparing the calculated photofragmentation spectra for various values of the triplet rate constant with the experimentally determined spectrum, Moore and co-workers[5] were able to "determine" the triplet rate constant. They found that the triplet rate constant which they determined increased more rapidly with excess energy than one would expect when considering that the total excess energy relative to the triplet barrier exceeds 1625 cm^{-1}. This k_t can, instead, be estimated from RRKM theory using a calculation based on a tight transition state for the $^3CH_2CO$ dissociation, as was also done in Ref. 5, or (not given here) could be estimated using a variational RRKM calculation.

As noted in Ref. 6, in the present case where PST does not give a good description of the singlet rate constant it may be preferable to use an improved calculation of the singlet rate constant in the expression $P(s)$ and then use the PST expression for $P(n|s)$. [The experimental energies considered in Ref. 5 were all below the threshold for vibrational

excitation of the singlet products and so the RRKM-based theory and PST yield the same expression for the quantity $P(n|s)$.] Perhaps, the failure of PST theory to describe the singlet rate constant accounts for the fact that the values determined for the effective number of triplet states W_t in the fitting procedure increased more rapidly than expected with increasing excess energy. As seen in the results presented in the earlier parts of this article, the present variational RRKM theory gives a good description of the singlet rate constant k_s and thus may be used to give an alternative "determination" of the triplet rate constants, with an additional assumption that the ratio $k_s^{\mathrm{RRKM}}/k_s^{\mathrm{PST}}$ is nearly constant over the entire energy range of a single photofragment excitation spectra. (Here, we take it to be that calculated at the threshold energy for the given CH_2 state.[38]) The results of this calculation are given in Table V, where it is seen that the RRKM-based method provides a k_t' which does not vary as rapidly over the entire energy range. However, there are still quite large fluctuations in the magnitude of this "experimentally determined" triplet number of states for $J = 0$.

VII. CONCLUDING REMARKS

The CH_2CO dissociation process is seen to present a good example of a dissociation process where the hindered rotor nature of a loose transition state causes a large difference between PST and RRKM theory. The present implementation of RRKM theory predicts a decrease by a factor of about 8 from the PST result for the singlet state rate constant at an excess energy of 6000 cm^{-1}, and the RRKM results for the rate constant are in good agreement with the experimental ones. In the present implementation an increased CO vibrational excitation is predicted relative to PST, in somewhat better agreement with experimental data.[10] Further experiments reducing the error bars and the degree of thermal averaging would be useful. A substantially increased vibrational excitation is predicted for the CH_2 fragment, this increase being particularly evident for each mode at energies just above the threshold for vibrational excitation of that particular mode. In addition, the same good agreement that was previously found between experimental photofragment excitation spectra at subvibrational[5,6] excitation energies and PST is shown to exist for the RRKM-based theory. In a subsequent work a comparison of these theories with the photofragment excitation spectra at energies exceeding the vibrational excitation of the products will be made.

The agreement between the present variational RRKM calculations on the rate constants and the experimental results may, of course, be partly fortuitous, because of the model nature of the potential energy surfaces. There is a real need for accurate potential energy surfaces in the transition state region (center-of-mass to center-of-mass separation distances of 2.6–3.4 Å between CH_2 and CO). The present variational RRKM method, in combination with the assumption of adiabatic vibrational and statistical rotational motions, appears to give an improved description of unimolecular dissociation rate constants and product state distributions, but the extent of agreement for the CO stretching vibrational excitation probabilities is still an open question, in virtue of the uncertainty in both the experimental data and the potential energy surface.

TABLE V. The triplet rate constants determined from RRKM and PST based fits of the experimental photofragment excitation spectra.

$^1CH_2$ state (J_{K_a,K_c})	k_t (PST)[a] ($\times 10^8\ s^{-1}$)	k_t' (RRKM)[a] ($\times 10^8\ s^{-1}$)
0_{00}	1.6(0.2)	1.6(0.2)
1_{01}	2.4(0.3)	2.4(0.3)
1_{11}	1.4(0.4)	1.4(0.4)
1_{10}	1.8(0.3)	1.8(0.3)
2_{02}	1.8(0.3)	1.8(0.3)
2_{12}	1.8(0.6)	1.8(0.6)
2_{11}	2.4(0.3)	2.4(0.3)
3_{03}	3.1(0.6)	2.2(0.4)
3_{12}	7.0(1.2)	3.7(0.6)
4_{13}	2.9(0.9)	1.1(0.3)
5_{13}	2.3(0.3)	0.8(0.1)
5_{14}	6.3(1.7)	1.8(0.5)
6_{16}	17.(6.)	4.5(1.5)

[a] The numbers in parentheses indicate estimated experimental uncertainties taken from Ref. 5.

ACKNOWLEDGMENTS

It is a pleasure to acknowledge the support of this research by the National Science Foundation. The authors would like to thank A. Hoffman, L. R. Khundkar, and A. H. Zewail for making the results of their picosecond spectroscopy experiments available to us prior to publication. S. J. K. also wishes to thank W. H. Green, Jr. and W. Nadler for helpful discussions.

APPENDIX

We consider (i) an elaboration of the PST expression for the number of states, for use in determining rate constants and product state distributions, when additional properties such as nuclear spin and parity with respect to inversion are conserved, and in section (ii) the effect of the initial thermal distribution of ketene and on the calculated rate constants and product state distributions.

1. PST expression for N_{EJ} and its use in determining k_{EJ}'s

The starting point for the quantum PST calculations is the number of states for a given energy E and total angular momentum J:

$$N_{EJ}^{\mathrm{PST}} = (2J+1) \sum_{j_{\mathrm{CH}_2}, j_{\mathrm{CO}}, l, k, K_{\mathrm{CH}_2}} N_v(E - E_l - E_{\mathrm{rot}})\Delta(J,k,l) \times \Delta(k, j_{\mathrm{CH}_2}, j_{\mathrm{CO}}), \quad \text{(A1)}$$

where j_{CH_2}, and j_{CO}, are the angular momentum quantum numbers for the CH_2 and CO fragments, respectively, k is the angular momentum quantum number for the vector sum of these two fragment angular momenta, $N_v(E)$ is the number of vibrational states with energy less than or equal to E, E_l is the energy of the orbital angular momentum l-dependent effective barrier for the centrifugal plus attractive potential, E_{rot} is the rotational energy of the two fragments, Δ

denotes a triangle inequality ($\Delta = 1$ if the inequality is fulfilled and $\Delta = 0$ otherwise), and K_{CH_2} is a quantum number which together with j_{CH_2} describes the rotational state of the CH_2 fragment.[39] The rotational energies for the CH_2 fragment were determined by diagonalization of the Hamiltonian for the asymmetric top[39] using the rotational constants given in Refs. 29 and 30. The rotational constant for the CO fragment was obtained from Ref. 28.

Equation (A1) is the correct expression to use when the only conserved quantities are E and J. However, Moore and co-workers[5,6] have shown through consideration of the threshold energies observed in their photofragment excitation spectra that nuclear spin is conserved[40] in the present case of the dissociation of ketene. Thus, in the present case two separate numbers of states should be considered, and two separate densities of reactant states, corresponding to the ortho and para nuclear-spin states of the reaction process should be calculated

$$N_{EJ}^{\text{ortho}} = (2J+1) \sum_{j_{CH_2} j_{CO} l k K_{CH_2}^{o}} [N_V(E - E_l - E_{\text{rot}}) \times \Delta(J,k,l)\Delta(k j_{CH_2} j_{CO})], \quad \text{(A2)}$$

$$N_{EJ}^{\text{para}} = (2J+1) \sum_{j_{CH_2} j_{CO} l k K_{CH_2}^{p}} [N_V(E - E_l - E_{\text{rot}}) \times \Delta(J,k,l)\Delta(k j_{CH_2} j_{CO})]. \quad \text{(A3)}$$

The number of allowed ortho *product* states at a given energy and angular momentum is found to be nearly identical to the number of allowed para *product* states (within about 1%). However, for low J the densities of *reactant* states for the ortho and para states are not as close and their ratio also depends on the value of J. Thus, for each initial J a different rate constant is predicted for each nuclear spin. The experimentally observed survival probability $Q(t)$, should then be given by

$$Q(t) = \sum_m P_m \exp(-k_m t), \quad \text{(A4)}$$

where P_m is the thermal probability of occupying a given total angular momentum and nuclear-spin state [e.g., see Eq. (A7) below],[41] and k_m is the rate constant for that state. The fit of $Q(t)$ to a single exponential is then given by the mean reaction time rate constant k_{MRT}[42]

$$\frac{1}{k_{\text{MRT}}} = \sum_m \frac{P_m}{k_m}. \quad \text{(A5)}$$

We have found that PST results for this rate constant k_{MRT} vary from 0.77 to 0.98 times that determined from a PST calculation in which the nuclear spin is ignored, when the rotational temperature was varied from 1 to 5 K. Similar arguments apply also to RRKM theory, although in the present implementation of RRKM theory the classical treatment of the rotational motions make it impossible to determine the ratio of the number of ortho to para states at the RRKM transition state. However, it is expected that when J is not too small these numbers of *ortho* and *para* states would be nearly identical, as was the case for PST. In the results plotted in Fig. 2 the above correction factor (which takes into account the distribution of rate constants due to the distribution for ortho–para ketene) is not included because of its small size and its dependence on temperature.

A measure of the nonexponentiality of the actual decay is given by the ratio μ_{-1}^2/μ_{-2}[42] where $\mu_{-1} = 1/k_{\text{MRT}}$ is the lowest order long-time moment of $Q(t)$ [Eq. (A5)[42]] and μ_{-2} is the second lowest order long-time moment. The latter[43] $\mu_{-2} \equiv \int_0^\infty dt(dQ/dt)t^2/2$ is given by

$$\mu_{-2} = \sum \frac{P_m}{k_m^2}. \quad \text{(A6)}$$

For the present case this ratio μ_{-1}^2/μ_{-2} is about 0.92, indicating that a single-exponential fit should be quite good. [Alternatively, a fit to a stretched exponential [i.e., $\exp(-k_\alpha t^\alpha)$ with an α of 0.92 could give a slightly improved fit to the survival probability $Q(t)$.[44]]

It has also been suggested[5,6,40] that parity with respect to inversion may also be conserved. In the present case test calculations indicated that conservation of this quantity had a negligible effect on the calculated rate constants. Thus, for simplicity, the restriction due to the conservation of parity was omitted in all of the calculations presented in Sec. IV.

2. Thermal average over initial distribution of ketene states

The product state distributions presented in Sec. IV for comparison with the experimental results of Ref. 10 involve a thermal average over the initial states of ketene, as do the predicted product rovibrational distributions presented in Figs. 3–11. The thermal averaging first requires consideration of the distribution of initial ketene states. Moore and co-workers[5,6] found that the supersonic jet expansion of the ketene molecules did not substantially change the distribution of the ketene spin states. Thus, the initial distribution of the ketene spin states retained the room temperature value of 3:1 ortho to para. The initial distribution of rotational and spin states can therefore be written as

$$P(J,K^o) = \frac{3}{4} \frac{(2J+1)\exp(-\beta E_{JK^o})}{\Sigma_{J,K^o}(2J+1)\exp(-\beta E_{JK^o})}, \quad \text{(A7)}$$

$$P(J,K^p) = \frac{1}{4} \frac{(2J+1)\exp(-\beta E_{JK^p})}{\Sigma_{J,K^p}(2J+1)\exp(-\beta E_{JK^p})}, \quad \text{(A8)}$$

where K^o and K^p are quantum numbers which specify the rotational state of ketene for a given J with ortho and para spin, respectively. $E_{JK^s}(s = o,p)$ is the rotational energy of a given J,K^s state and β is $1/k_B T$ where k_B is Boltzmann's constant and T is the rotational temperature of the molecular beam.

The predicted product state distribution is then determined through a summation over the initial rotational states of a product of two factors:

$$P_E(i,t) = \sum_{J,s,K^s} P(J,K^s) P_E(i,t|J,K^s), \quad \text{(A9)}$$

where $P(J,K^s)$ is the probability of having an initial state (J,K^s) of ketene [Eqs. (A7)–(A8)], and $P_E(i,t|J,K^s)$ is the conditional probability of occupying vibrational state i and rotational state t of the products, when the ketene is in the state (J,K^s), and is given by

$$P_E(i,t\,|J,K^s) \propto \frac{N^{\dagger}_{E(J,K^s)J'i}}{\Sigma_i N^{\dagger}_{E(J,K^s)J'i}} \frac{N^{\mathrm{PST}}_{E(J,K^s),J',i,t}}{\Sigma_t N^{\mathrm{PST}}_{E(J,K^s),J',i,t}} \times \sigma(J',K^{s'} \leftarrow JK^s;h\nu). \quad \text{(A10)}$$

Here, the $N^{\dagger}_{EJi}$ may be determined from either PST or RRKM theory to give either "PST" distributions or "RRKM" distributions, and $\sigma(J',K^{s'} \leftarrow JK^s;h\nu)$ is the dipole transition probability. The use of the PST number of states in the second term on the right-hand side of Eq. (A10) arises from the assumption (in the RRKM-based theory of Ref. 21) that for a given vibrational state i of the fragments the rotational distribution is given by the statistical PST distribution. The dipole transition probability is approximated here via symmetric top Hoïl–London factors as in Ref. 5.

Equation (A10) was used directly in the determination of the PST vibrational–rotational distributions presented in Figs. 3–11 (with the additional constraint of parity conservation as described in Ref. 5). However, one simplification was employed in the determination of the RRKM vibrational–rotational distributions: This simplification involved the determination of the $N^{\dagger}_{EJ'i}$'s only for $(J,K) = (3,0)$ rather than for each individual (J,K). This simplification was introduced since the $\pm$ 5% to 10% error bars of the present Monte Carlo calculations are greater than any possible difference which would arise from the small range of (J,K) values in a 3 K thermal distribution.

Equation (A10) was also used for the calculation of the CO vibrational excitation probability resulting from the photodissociation of the ketene molecules with a room temperature distribution. In this case however the conservation of nuclear spin was not important, because of the large distribution of initial J's, K's and vibrational states present. Also, the dipole transition factor was not considered in these calculations. This large distribution also necessitated the use of approximate summation/integration techniques in performing the summation over the initial distribution of ketene states. The J summation was thus approximated as an integral. Gauss–Laguerre integration was then applied to the J integral, and gridded sums with interpolation formulas were used for the K and vibrational states sums.[13]

[1] C. X. W. Qian, M. Noble, I. Nadler, H. Reisler, and C. Wittig, J. Chem. Phys. **83**, 5573 (1985), and references cited therein.

[2] L. R. Khundkar, J. L. Knee, and A. H. Zewail, J. Chem. Phys. **87**, 77 (1987).

[3] L. J. Butler, T. M. Ticich, M. D. Likar, and F. F. Crim, J. Chem. Phys. **85**, 2331 (1986); T. M. Ticich, T. R. Rizzo, H. R. Dübal, and F. F. Crim, J. Chem. Phys. **84**, 1508 (1986), and references cited therein.

[4] N. F. Scherer and A. H. Zewail, J. Chem. Phys. **87**, 97 (1987), and references cited therein.

[5] I.-C. Chen, W. H. Green, Jr., and C. B. Moore, J. Chem. Phys. **89**, 314 (1988).

[6] W. H. Green, Jr., I.-C. Chen, and C. B. Moore, Ber. Bunsenges, Phys. Chem. **92**, 389 (1988).

[7] A. H. Zewail *et al.* (to be published).

[8] W. H. Green, Jr., A. J. Mahoney, C.-k. Cheng, and C. B. Moore (private communication).

[9] A. Kiermeier, H. J. Neusser, and E. W. Schlag, Z. Naturforsch. Teil A **42**, 1399 (1987); A. Kiermeier, H. Kühlewind, H. J. Neusser, E. W. Schlag, and S. H. Lin, J. Chem. Phys. **88**, 6182 (1988).

[10] D. J. Nesbitt, H. Petek, M. F. Foltz, S. V. Filseth, D. J. Bamford, and C. B. Moore, J. Chem. Phys. **83**, 223 (1985).

[11] H. Bitto, D. R. Gwyer, W. F. Polik, and C. B. Moore, Far. Discuss. Chem. Soc. **81**, 149 (1986).

[12] P. Pechukas and J. C. Light, J. Chem. Phys. **42**, 3281 (1965); P. Pechukas, R. Rankin, and J. C. Light, J. Chem. Phys. **44**, 794 (1966); C. Klotz, J. Phys. Chem. **75**, 1526 (1971).

[13] D. M. Wardlaw and R. A. Marcus, Chem. Phys. Lett. **110**, 230 (1984); D. M. Wardlaw and R. A. Marcus, J. Chem. Phys. **83**, 3462 (1985); D. M. Wardlaw and R. A. Marcus, J. Phys. Chem. **90**, 5383 (1986); D. M. Wardlaw and R. A. Marcus, Adv. Chem. Phys. **70**, 231 (1988).

[14] A. F. Wagner and D. M. Wardlaw, J. Phys. Chem. **92**, 2462 (1988); E. E. Aubanel and D. M. Wardlaw, *ibid.* **93**, 3117 (1989); W. L. Hase and D. M. Wardlaw, in *Gas Phase Biomolecular Processes* (Royal Society of Chemistry, London, in press).

[15] C. J. Cobbs and J. Troe, J. Chem. Phys. **83**, 1010 (1985); S. W. Benson, Can. J. Chem. **61**, 881 (1983); W. L. Hase and R. J. Duchovic, J. Chem. Phys. **83**, 3448 (1985), and references cited therein.

[16] S. J. Klippenstein, L. R. Khundkar, A. H. Zewail, and R. A. Marcus, J. Chem. Phys. **89**, 4761 (1988).

[17] S. J. Klippenstein, Ph.D. thesis, California Institute of Technology, 1988.

[18] S. J. Klippenstein and R. A. Marcus, J. Phys. Chem. **92**, 3105 (1988).

[19] S. J. Klippenstein and R. A. Marcus, J. Phys. Chem. **92**, 5412 (1988).

[20] M. Quack and J. Troe, Ber. Bunsenges Phys. Chem. **78**, 240 (1974); J. Troe, J. Phys. Chem. **88**, 4375 (1984), and references cited therein.

[21] R. A. Marcus, Chem. Phys. Lett. **144**, 208 (1988).

[22] W. D. Allen and H. F. Schaefer III, J. Chem. Phys. **84**, 2212 (1986); **89**, 329 (1988).

[23] P. R. Bunker, P. Jensen, W. P. Kraemer, and R. Beardsworth, J. Chem. Phys. **85**, 3724 (1986).

[24] C. C. Hayden, D. M. Neumark, K. Shobatake, R. Sparks, and Y. T. Lee, J. Chem. Phys. **76**, 3607 (1982).

[25] The present setting of the orientation factor to zero when the magnitude of any of the angular deviations is greater than $\pi/2$ was not done in the model surfaces of Refs. 13, 16, and 17.

[26] C. B. Moore and G. C. Pimentel, J. Chem. Phys. **38**, 2816 (1963).

[27] P. D. Mallinson and L. Nemes, J. Mol. Spectrosc. **59**, 470 (1976).

[28] K. P. Huber and G. Herzberg, *Constants of Diatomic Molecules* (Van Nostrand Reinhold, New York, 1979).

[29] D. Feldmann, K. Meier, R. Schmiedl, and K. H. Welge, Chem. Phys. Lett. **60**, 30 (1978).

[30] H. Petek, D. J. Nesbitt, C. B. Moore, F. W. Birss, and D. A. Ramsay, J. Chem. Phys. **86**, 1189 (1987); H. Petek, D. J. Nesbitt, P. R. Ogilby, and C. B. Moore, J. Phys. Chem. **87**, 5367 (1983).

[31] Y. P. Varshni, Rev. Mod. Phys. **29**, (1957); D. Steele, E. R. Lippincott, and J. T. Vanderslice, *ibid.* **34**, 239 (1962).

[32] It was not possible to obtain a simultaneous fit to all three of the assumed bonding potential parameters $r_{e,CC}$, β_{CC}, and D_{CC}. For this reason, a value of 1.15 Å was chosen for the parameter $r_{CC}^{e,\mathrm{eff}}$ in rough analogy with the values chosen for the corresponding parameters in previous studies (Refs. 13 and 16). The two parameters $\beta_{CC}^{\mathrm{eff}}$ and D_{CC}^{eff} were then varied until the minimum of the total potential (that is, the sum of the bonding plus nonbonding potential) was equivalent to the value of the assumed potential at r_{CC} distances of 2.1 and 2.3 Å. (These values of r_{CC} roughly correspond to $R^{\dagger} = 2.8$ and 3.0 Å.)

[33] W. L. Jorgensen and C. J. Swenson, J. Am. Chem. Soc. **107**, 569 (1985).

[34] For example, see J. R. Barker, J. Phys. Chem. **91**, 3849 (1987) for a study of the effect of anharmonicities and mode–mode coupling on the density of states for the molecules H_2O and CH_2O. They find that for CH_2O at an energy of 30 000 cm^{-1} the effect of anharmonicities and mode–mode coupling is to increase the density of states by a factor of about 1.5.

[35] W. H. Miller, J. Chem. Phys. **65**, 2216 (1976); J. O. Hirschfelder, E. Wigner, *ibid.* 7, 616 (1939); W. J. Chesnavich, L. Bass, T. Su, and M. T. Bowers *ibid.* **74**, 2228 (1981).

[36] An alternative expression for the effective number of states has also been derived. E. Pollak and P. Pechukas, J. Chem. Phys. **70**, 325 (1979); E. Pollak, M. S. Child, and P. Pechukas, *ibid.* **72**, 1669 (1980). Due to the occurence of a quite large value for the maximum in the number of states for certain situations this expression resulted for the present system in unphysical values for the vibrational distributions and so is not further considered here.

[37] S. N. Rai and D. G. Truhlar, J. Chem. Phys. **79**, 6046 (1983).

[38] In performing a fit to the experimental data this variance could actually be taken into account. However, in the present case we are only interested in illustrating the possible magnitude that the effect may have, and so the above approximation should suffice.

[39]I. N. Levine, *Molecular Spectroscopy* (Wiley, New York, 1975).
[40]For a theoretical discussion of nuclear spin and other conservation rules see, M. Quack, Mol. Phys. **34**, 477 (1977); Stud. Phys. Theor. Chem. **23**, 355 (1983).
[41]This definition of the P_m assumes that the experimental probability for observing a given state is independent of the total angular momentum and of the nuclear-spin state. For those cases where the observation probability depends on these quantities then P_m should be multiplied by the appropriate observation probabilities.
[42]W. Nadler and R. A. Marcus, Chem. Phys. Lett. **144**, 24 (1988). This MRT $1/k_{\mathrm{MRT}}$ is defined as $-\int_0^\infty dt(dQ/dt)$. The latter equals $\int_0^\infty dt\, Q(t)$ and in conjunction with Eq. (A4) yields Eq. (A5).
[43]K. Schulten, A. Brünger, W. Nadler, and Z. Schulten, in *Synergetics—From Microscopic to Macroscopic Order*, edited by E. Frehland (Springer, Berlin, 1984), pp. 80–89.
[44]In this range of the ratio μ^2_{-1}/μ_2 the parameter α for a stretched exponential is nearly identical to the above ratio. W. Nadler (private communication).